Available online at www.sciencedirect.com

SciVerse ScienceDirect

Ceramics International 39 (2013) 4055–4062

CERAMICS INTERNATIONAL

www.elsevier.com/locate/ceramint

Viscosity, fragility and structure of Na_2O–CaO–Al_2O_3–SiO_2 glasses of increasing Al/Si ratio

Jinshu Cheng, Zifan Xiao*, Kun Yang, Hao Wu

State Key Laboratory of Silicate Materials for Architectures, Wuhan University of Technology, Wuhan 430070, China

Received 16 August 2012; received in revised form 25 October 2012; accepted 27 October 2012
Available online 5 November 2012

Abstract

The research and development of a new float glass with higher content of Al_2O_3 is essential for the commercial flat glass. The study on the workability and kinetic fragility of Na_2O–CaO–Al_2O_3–SiO_2 glass melts with different Al/Si ratios has been linked with the structure. The viscosities as a function of temperature for glass melts were derived on the basis of Vogel–Fulcher–Tamman (VFT) equation. Some characteristic temperatures and four characteristic temperature intervals of forming process in tin bath were estimated. The results showed that: adding 12 wt% Al_2O_3 substitute for SiO_2, the melting point (*Tm*) increased about 35 K, entire temperature interval in tin bath narrowed down about 20 K, the shortening of workability was mainly reflected in the viscosity range of $10^{5.75}$–10^{10} Pa s, the fragility index *m* increased by 15%. It reveals an inverse correlation between the workability and the fragility. The structural changes on the tetrahedron structural unit Q^n ($n=1, 2, 3, 4$) were obtained by using Raman spectroscopy. Our analysis indicates that: the number of *NBO* reducing and a more polymerized structure with adding Al/Si ratios are responsible for the increase of viscosity; the tetrahedral distortion, a decrease of Q^3/Q^2 in the Q^n species, is responsible for the increase of fragility.

Keywords: Viscosity; Workability; Kinetic fragility; Structure

1. Introduction

Glass viscosity is one of the key properties for melting, fining, processing optimization, glass formation and annealing process. Commercial forming method requires very precise control of the viscosity throughout the glass forming process in order to achieve high throughput and high yield of acceptable products [1–5]. Most data on viscosity have been published for these systems [6–9], such as silica glass, soda–lime–silica glass, borosilicate glass, etc. The soda–lime–silica ternary system has been one of the most studied during the last century and adopted as the main system of commercial glass so far. The content of Al_2O_3 in these glasses is often restricted below 2 wt% in order to avoid some problems in production, such as: poor uniformity, glass stripes and stones, etc. However, this stereotypical chemical composition has been a restraining factor on the improvement of physicochemical properties nowadays.

Besides the viscosity, the workability of glass melt is another key property in glass forming process. Naming in industrial production, glass melt which has a large working range is often referred to "long glass"; there against the one is called "short glass". Angell [10–12] proposed a classification of liquids between strong and fragile. Glass-forming liquids are classified as either "strong" or "fragile" depending on whether they display an Arrhenius or non-Arrhenius dependence of dynamics on temperature respectively. However, the relationship between workability and fragility for glass melts remains unclear.

Spectroscopic techniques, such as magic-angle spinning–nuclear magnetic resonance (MAS–NMR) and Raman, have allowed researchers to obtain insights into the glass structure. For example, ^{27}Al and ^{29}Si MAS–NMR studies have shown that the addition of Al_2O_3 to alkali silicate glasses causes non-bridging oxygen sites (NBO sites) to be converted to bridging-oxygen (BO) sites as the additional

*Corresponding author. Fax: +86 27 87860801.
E-mail address: xzf586586@163.com (Z. Xiao).

0272-8842/$ - see front matter © 2012 Elsevier Ltd and Techna Group S.r.l. All rights reserved.
http://dx.doi.org/10.1016/j.ceramint.2012.10.258

oxygen required for Al to occupy a tetrahedral coordination is removed from the NBO site [13–16]. It means that formation of $[AlO_4]$–Na strengthens the structural network by increasing bond connectivity via formation of Al–O–Si linkages. The structural changes in glass melts may be responsible for the variation on the viscosity and fragility.

Here we realize that the research and development of a new float glass with higher content of Al_2O_3 is an important demand for the industry of construction and transportation. The viscosity data on this Na_2O–CaO–Al_2O_3–SiO_2 system glass is the most significant in determining the glass forming process. This paper focuses on the effect of Al/Si ratio on the viscosity, fragility and structure of the Na_2O–CaO–Al_2O_3–SiO_2 system glasses. Raman spectroscopy is used to probe the structure of glass melts, in order to further reveal a relationship between the melts properties and the structure.

2. Experimental

Batch compositions $(72-X)SiO_2$–$X(X=1, 5, 9, 13)$ Al_2O_3–14.5Na_2O–8.5CaO–4MgO (wt%) were mixed from reagent grade SiO_2, Al_2O_3, Na_2CO_3, $CaCO_3$, MgO, and then melted in corundum crucibles in electric furnace at the temperature between 1773–1853 K for 3 h. A part of melt was poured into a pre-heating stainless steel mould to form, and then annealed for 1 h at below 50 K the glass transition temperature T_g determined by dilatometry. Regular bulk glass samples (4 mm × 4 mm × 30 mm) were prepared for dilatometry test. The residual melt was poured into water and dried for 24 h to obtain glass frit for testing viscosity and structure. The glass samples were labeled with a short word 1#, 5#, 9# and 13#. The chemical compositions of all samples were determined by the wavelength dispersive X-ray fluorescence (WDXRF) using an Axios X-ray spectrometer, shown in Table 1.

The viscosity of glass frit quenched in water was measured with a rotating crucible viscometer (Model Rheotronic II). The viscometer was calibrated for 5 times with a standard quartz glass before testing. The standard measurement error is less than 5% log units. About 200 g of glass frit was added into a Pt crucible and placed into the furnace set at 1733 K. The viscometer spindle was placed in the center of the crucible. The furnace was set to the required ramp/soak schedule, and digital data collection and recording began. The dilatometric experiments were performed in a horizontal dual-rod dilatometer (Model DIL 402) at heating rate of 10 K/min and the quartz glass (provided by DGG) was looked as standard. The Raman spectra of all samples were recorded using an INVIA confocal microRaman spectrometer (RENISHAW) equipped with a CCD detector. The 514.5 nm light from Ar^+ laser was chosen for sample excitation. The spectral resolution of the Raman spectrometer was 1–2 cm^{-1} and the measurement range was in 200–1400 cm^{-1}.

3. Results

3.1. Viscosity and workability

As an empirical curve-fitting tool, the Vogel–Fulcher–Tamman (VFT) equation,

$$\log \eta = A + B/(T - T_0) \quad (1)$$

has the advantages of simplicity and quite wide applicability [8,9]. The high-viscosity data (in Pa s) were obtained from the rotating crucible viscometer. While the T_g and T_s measured by dilatometry (Table 1) can stand for the low-viscosity data of $10^{12.4}$ Pa s and 10^{10} Pa s respectively [17,18]. The viscosities of all samples over the temperature interval between the T_g ($10^{12.4}$ Pa s) and the T_m (10 Pa s) were well fitted by the VFT equation (Fig. 1) and the constants A, B and T_0 have been evaluated (Table 2). It seems the most appropriate equation for using in this paper (all R^2 above 99.9%). Some characteristic temperature points in glass technology [17,18] were calculated from the VFT equation and listed in Table 2. It is obvious that all characteristic temperatures increase with the Al/Si ratios increasing (Fig. 2).

Eric Le Bourhis [17] has proposed the workability of the container glass to be the temperature interval between the working point (10^3 Pa s) and the Littleton's softening point ($10^{6.65}$ Pa s). It is well known that the float process introduced by Pilkington Brothers Ltd. in the 1950s is a revolution for the glass industry. As forming process in tin bath can offer very good optical quality without requiring any further operation, the workability of the float glass should be defined as the entire temperature interval in tin bath, i.e. viscosities between $10^{2.7}$ and 10^{10} Pa s. Furthermore, there are mainly four process sections in tin bath [19]: the flatting-polishing section ($10^{2.7}$–$10^{3.2}$ Pa s), the slow cooling section ($10^{3.2}$–$10^{4.25}$ Pa s), the forming section ($10^{4.25}$–$10^{5.75}$ Pa s) and the hardening section

Table 1
Chemical composition (wt%) determined by WDXRF analysis and Tg, T_s (K) determined by dilatometry for all glass samples.

Samples no.	SiO_2	Al_2O_3	Na_2O	CaO	MgO	L.O.I	Al/Si	T_g	T_s
1#	71.720	1.158	13.721	9.333	3.620	0.447	0.016	826.3 ± 1.1	888.6 ± 0.6
5#	67.604	5.284	13.551	9.839	3.315	0.407	0.078	843.3 ± 1.5	901.6 ± 0.3
9#	63.138	8.999	14.018	9.194	4.040	0.547	0.143	854.2 ± 1.3	909.5 ± 0.4
13#	59.694	13.451	13.659	9.417	3.686	0.381	0.225	870.7 ± 0.9	918.3 ± 0.2

($10^{5.75}$–10^{10} Pa s). Table 2 shows that all temperature intervals narrow down with increasing the Al/Si ratios.

3.2. Kinetic fragility

$$m = \frac{d(\log \tau)}{d(T_g/T)}\Big|_{T=T_g} \quad (2)$$

$$m = \frac{d(\log \eta)}{d(T_g/T)}\Big|_{T=T_g} \text{ and}$$

$$\log \eta = A + \frac{B}{(T-T_0)} \rightarrow m = \frac{B}{T_{12.4}\left(1-\left(T_0/T_{12.4}\right)\right)^2} \quad (3)$$

Kinetic fragility has been studied for a broad variety of anhydrous inorganic and organic liquids [10–12,20–23]. A strong liquid shows a linear variation in a log η versus T_g/T diagram, while this linear relation is not preserved in a fragile liquid. The viscosities of all glass melts have been plotted as a function of T_g/T (Fig. 3), in addition molten SiO_2 is known as the strongest liquid. The strongest liquid of the glass investigated in this paper was the 1#, while the most fragile liquid was the 13#. Fragility itself is defined as the slope of the log η versus T_g/T curve at the glass transition temperature ($T_{12.4}=T_g$), Eq. (2). We have utilized the Eq. (1) and (2) equals and estimated the fragility index m from Eq. (3), in Table 2.

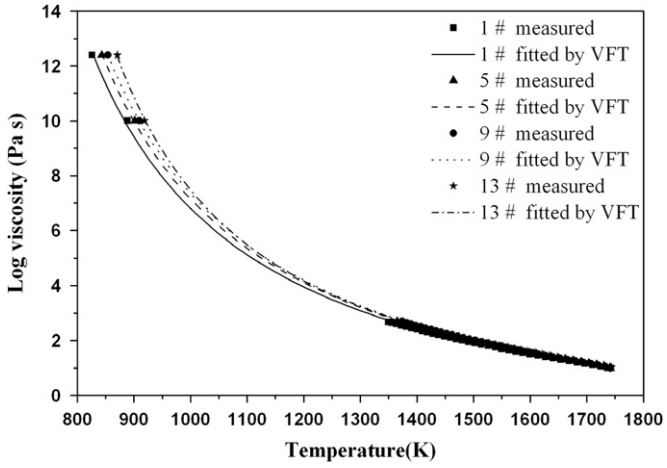

Fig. 1. Viscosity as a function of temperature for glass samples fitted by the VFT equation.

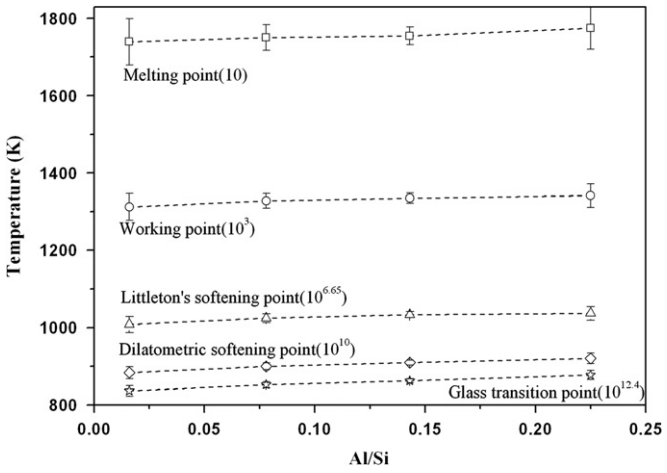

Fig. 2. Character temperature points of glass melts versus Al/Si.

Table 2
Parameters for VFT equation, fragility index from Eq. (3), some characteristic temperatures and four characteristic temperature intervals of forming process in tin bath for all glass samples.

Samples no.	**1#**	**5#**	**9#**	**13#**
VFT equation parameter				
A	-2.62 ± 0.08	-2.67 ± 0.04	-2.67 ± 0.03	-2.24 ± 0.07
B	4351.04 ± 39.84	4397.02 ± 57.22	4369.30 ± 39.84	3770.67 ± 83.44
T_0	538.7 ± 5.6	552.4 ± 3.1	564.4 ± 2.2	612.3 ± 4.8
R^2	0.9996	0.9998	0.9999	0.9999
Fragility index m from Eq. (3)	41.10 ± 0.72	41.71 ± 0.41	42.48 ± 0.30	47.20 ± 0.86
Characteristic temperature (K)				
Melting point (10)	1739.1 ± 60.1	1750.1 ± 33.2	1754.3 ± 23.1	1774.5 ± 55.1
Point into the tin bath (10^2)	1479.5 ± 43.9	1493.7 ± 34.3	1499.6 ± 16.9	1500.7 ± 38.8
Working point (10^3)	1312.3 ± 34.7	1327.7 ± 19.3	1334.7 ± 13.4	1331.3 ± 30.2
Littleton's softening's softening point ($10^{6.65}$)	1007.8 ± 20.6	1024.1 ± 11.5	1033.1 ± 8.0	1036.3 ± 17.5
Dilatometric softening point (10^{10})	883.3 ± 15.8	899.4 ± 8.8	909.2 ± 6.1	920.3 ± 13.4
Glass transition point ($10^{12.4}$)	828.3 ± 13.9	844.2 ± 7.8	854.3 ± 5.4	869.8 ± 11.7
Characteristic temperature interval of forming process in tin bath (K)				
Flatting and polishing section ($10^{2.7}$–$10^{3.2}$)	70.2	69.7	69.3	70.0
Slow cooling section ($10^{3.2}$–$10^{4.25}$)	114.1	113.6	112.9	112.0
Forming section ($10^{4.25}$–$10^{5.75}$)	113.4	113.2	113.4	109.0
Hardening section ($10^{5.75}$–10^{10})	174.9	175.1	174.0	163.7
Total	472.5	471.6	468.6	454.6

3.3. Raman spectra

It can be observed from Fig. 4 that there was some distinct variations in Raman spectral curve of the investigated glasses. In order to discern the variations, a dashed line has been added into the curve. It indicates the spectral shift from the band near 1100 cm^{-1} for glass sample 1# and draws the eye to the lower frequency shift as a function of addition Al_2O_3 substitute for SiO_2.

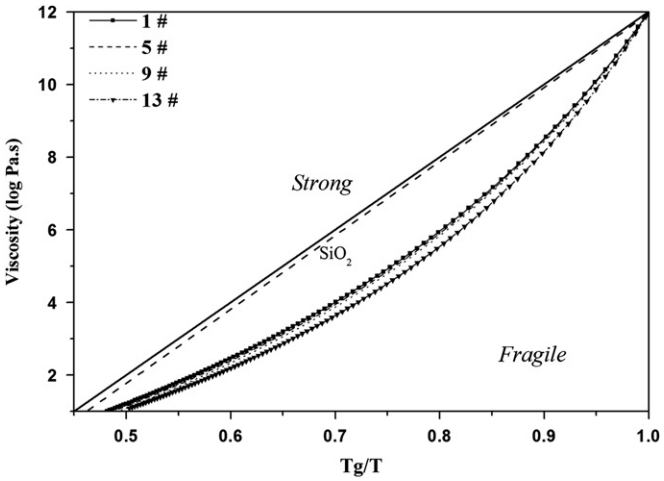

Fig. 3. Fragility plot visualizing viscosity of all glass samples versus T/Tg.

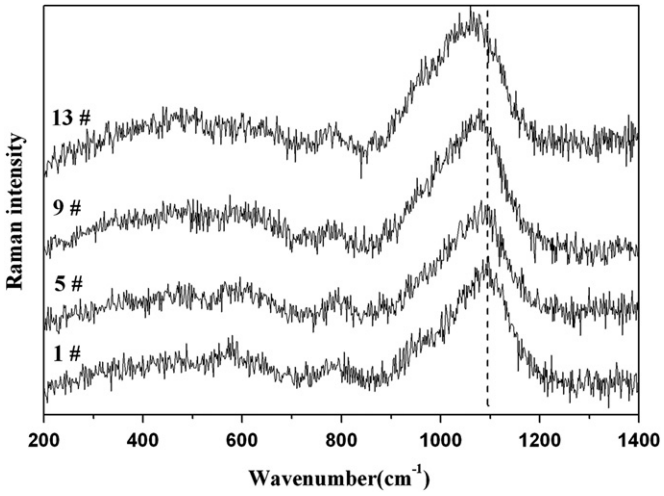

Fig. 4. Raman spectra at room temperature of all glass samples.

The high frequency region (900–1200 cm^{-1}) of Raman spectra was deconvoluted with the technique described by Neuville [24,25] for all glass samples, the fitting results are given in Fig. 5. It can be observed that there are four bands at or near 950, 1020, 1090 and 1150 cm^{-1}, the assignments of these bands mainly correspond to $Si–O^-$ stretch vibrations in specific structural units [24–30]: Q^1 (NBO/T=3, dimmer), Q^2 (NBO/T=2, chain), Q^3 (NBO/T=1, sheet), Q^4 (three-dimensional network), respectively. Frequencies, areas, area% of Raman bands obtained from the deconvolution fits were listed in Table 3.

4. Discussion

4.1. Viscosity and workability

The results presented here demonstrate that the addition of Al_2O_3 substitute for SiO_2 in $Na_2O–CaO–Al_2O_3–SiO_2$ system glass increases the viscosity of glass melts, which is in good agreement with the finding of [13,15,16]. Adding 12 wt% Al_2O_3 substitute for SiO_2, the melting point increased about 35 K. It indicates that the glass melting furnaces need to have a higher performance requirement in order to guarantee the high quality of glass products. The T_g point also increased about 40 K.

Adding 12 wt% Al_2O_3 substitute for SiO_2, entire temperature interval in tin bath narrowed down about 18 K, i.e. the workability of glass melts got shorter with increasing Al/Si

Table 3
Frequencies (F), areas (A), area% (A%) of Raman bands obtained from the deconvolution fits.

Samples no.	1#	5#	9#	13#
F1	942.92	945.83	940.15	944.85
F2	1012.87	1014.85	1009.02	1019.22
F3	1089.03	1086.64	1082.73	1086.63
F4	1147.96	1151.92	1149.91	1148.88
A1	8410.14	6993.93	8232.07	6948.13
A2	17593.41	19405.63	27035.69	32867.70
A3	39882.48	33841.57	42137.41	32835.20
A4	6562.02	6187.82	7194.11	9521.22
A1%	11.61	10.53	9.73	8.46
A2%	24.28	29.21	31.96	40.00
A3%	55.05	50.95	49.81	39.96
A4%	9.06	9.31	8.50	11.59

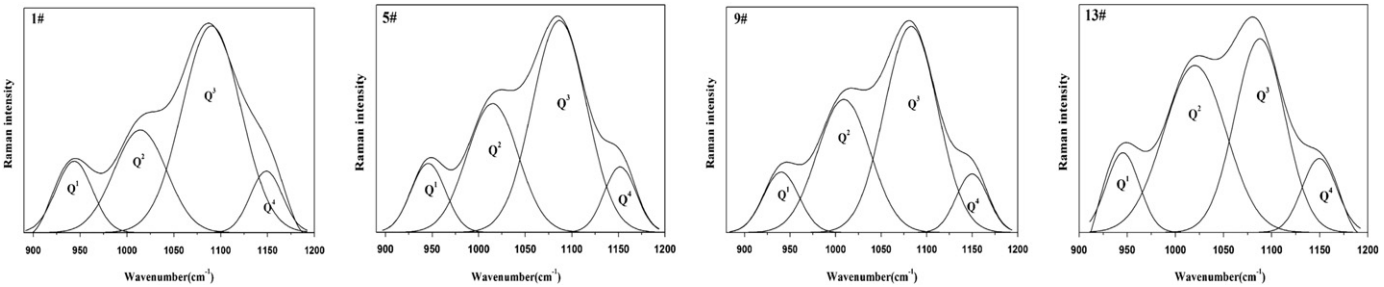

Fig. 5. Deconvoluted Raman spectrum at 900–1200 cm^{-1} for all glass samples.

ratios. In other words, the viscosity increasing from $10^{2.7}$ to 10^{10} Pa s can be achieved in a temperature range of about 455 K in sample 13#, which is less than the sample 1# (473 K). However, we found that very little change occurred in the flatting–polishing section and the slow cooling section. The temperature interval of the forming section, which was the main section for controlling the glass thickness, narrowed down with only 5 K. Hence, the shortening of workability is mainly reflected in the hardening section. It can be related to the structural breaks of glass network in this viscosity interval ($10^{5.75}$–10^{10} Pa s) [17]. This finding suggests that the structural break along with the viscosity increasing can be accomplished in a more narrow temperature range in the glass melts with shorter workability.

4.2. Relation between fragility and workability

In Fig. 6, we show that there is an inverse correlation between the workability and the fragility index m, as the Al/Si ratios are increased. The fragility index m increased by 15% when the temperature interval in tin bath narrowed down about 18 K. So we propose that the fragility can be objectified by the entire temperature interval in tin bath. As mentioned in Section 3.1, the change of workability mainly occurs in the hardening section. In contrast to others, this section is more close to T_g, which is the reference temperature point of the fragility. Therefore the fragility of glass melts also can be related to the structural break of glass network in this viscosity interval ($10^{5.75}$–10^{10} Pa s), namely the structural break along with the viscosity increasing can be easier to accomplish in a more fragility liquid.

Fragility reflects the degree of order within a glass melt [9–12,21,22]. In general a strong melt has a high degree of short range order, whereas a fragile melt often lacks directional bonds and thus does not have a well defined short range order. It indicates that the structure characteristic in glass sample 13# has the most disorder in short-range. A more detailed studying on the structure is following in next section.

4.3. Q^n species and tetrahedra distortion

Fraction and content of structure units Q^n ($n=1, 2, 3, 4$) were calculated on the basis of the theory proposed by Umesaki et al. [29], summarized in Table 4. It shows that the contents of Q^1 and Q^4 species occur in small amounts and Q^3 and Q^2 species are the main structural units in this system. In addition, the band of Raman spectra at 1020 cm^{-1} can be assigned to two parts [3,28]: (i) Si–O^- stretching vibration in tetrahedra with two NBO per tetrahedron; (ii) Al–O^- vibration in $[AlO_4]^-$ tetrahedrons. The latter enhanced the band assigned to Q^2 with increasing the Al/Si ratio. However, since we have not yet been

Table 4
Fraction (X^n%), content (Q^n) of structure units, Q^3/Q^2 ratio, fraction of non-bridging oxygen and average number of NBO per tetrahedron.

Samples NO.	1#	5#	9#	13#
X^1%	13.35	12.11	11.19	9.72
X^2%	24.77	29.80	32.60	40.80
X^3%	57.25	52.98	50.76	41.56
X^4%	4.63	5.11	5.45	7.92
Q^1	9.64	8.99	8.42	7.61
Q^2	17.89	22.13	24.53	31.93
Q^3	41.35	39.34	38.20	32.52
Q^4	3.34	3.80	4.10	6.20
Q^3/Q^2	2.31	1.78	1.56	1.02
NBO/NBO+BO (%)	60.72	59.78	57.96	57.59
NBO/tetrahedron	1.45	1.40	1.35	1.31

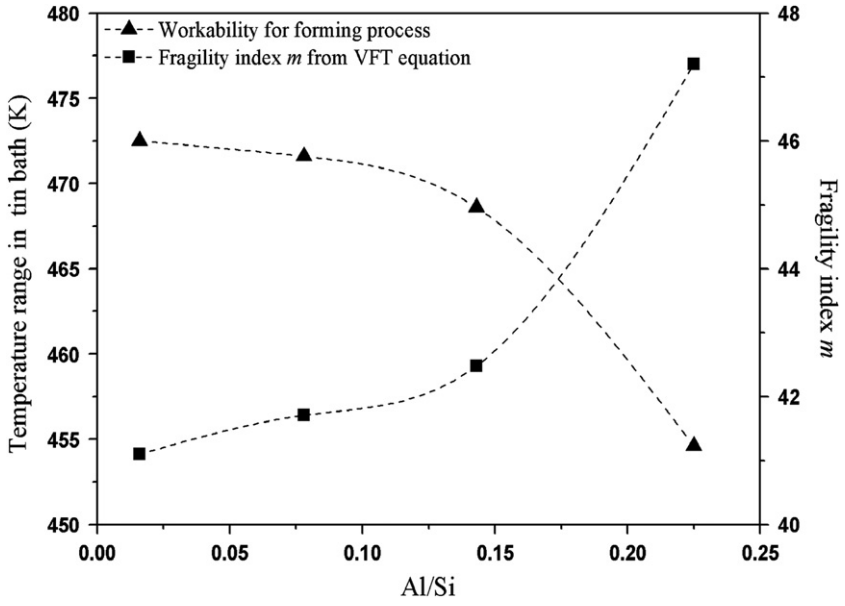

Fig. 6. Al/Si dependence of workability in forming process, fragility index m.

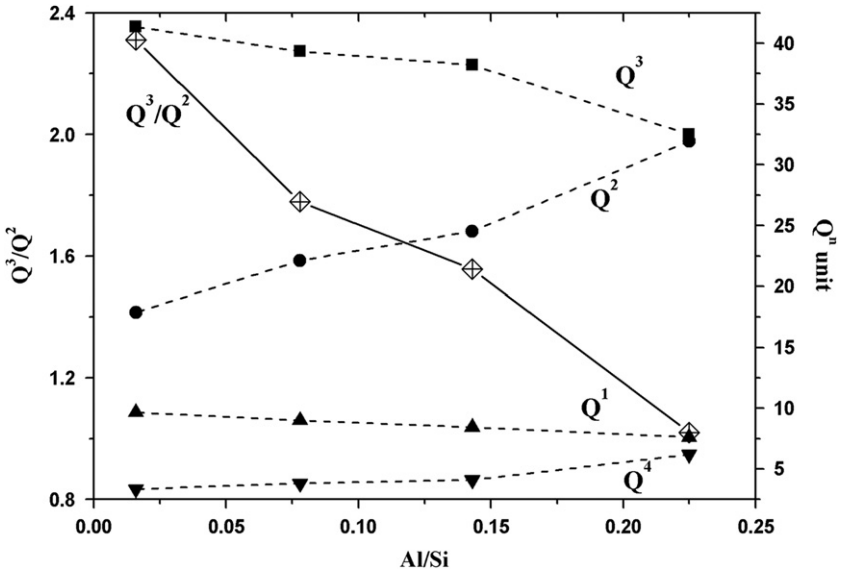

Fig. 7. Al/Si dependence of Q^n structure units and Q^3/Q^2 ratio.

able to extract this part from the peak fitting results, no quantifying for the $[AlO_4]^-$ tetrahedrons.

Interestingly, our present data show that the contents of Q^2 and Q^4 units are positively correlated with Al/Si ratio, whereas the contents of Q^1 and Q^3 units both decrease with adding Al_2O_3 (Fig. 7). The variation of Q^n species in investigated glass can be described simply as: $Q^1+Q^3 \rightarrow Q^2+Q^4$, in a manner similar to the studies of Bjorn Mysen [3,31]. The finding that Q^3/Q^2 ratio decreased with adding Al may correspond to an increase of the tetrahedra distortion. This assumption can be confirmed by molecular dynamics [32–34]. They show that Si–BO average distances are shorter than Si–NBO average distance, suggesting that Q^2 units are more distorted than Q^3 or Q^4 units. Moreover, the fact that the volume of $[AlO_4]^-$ tetrahedrons is larger than $[SiO_4]$ can be regarded as another reason for the tetrahedra distortion. Just confirmed in Section 3.2, the characteristic structure in sample 13# has the most disorder in short-range. It indicates that this tetrahedra distortion can answer for the short-range disorder in glass structure. Consequently we make a conclusion that the addition of Al_2O_3 substitute for SiO_2 induces an increase of the tetrahedra distortion, with a decrease of Q^3/Q^2 ratio in Q^n species, leading to an increase of fragility in glass melts. This finding and the reports of Neuville are in common. Neuville [24] suggested the addition CaO substitute for Na_2O to the silicate melts produces an increase of the fragility of the liquid and a decrease of the Q^3/Q^2 ratio observed with Raman spectroscopy.

4.4. NBO and network polymerization

Hamlton and Pantano [35] proposed the connectivity numbers to characterize the silicate glass structure on the basis of some assumptions. The NBO content in the alkali–silicate determined by the ESCA method,

$$\mathrm{NBO} = \sum Q^n(4-n) \tag{4}$$

proved that the BO and NBO total content in the alkali–silicate glass calculated by this method is quite accurate. Umesaki et al. [29] also investigated the structure of alkali–silicate glass using a Raman spectrometer, and the

$$\mathrm{NBO}/T = \sum Q^n(4-n)/[\mathrm{Si}+\mathrm{Al}] \tag{5}$$

was calculated. Just mentioned, it is difficult to accurately quantify the fractions of Si–O^- and Al–O^- vibration in tetrahedra Q^2. Based on the conventional model, every Al ion (up to the ratio Na/Al=1) enters into the network and eliminates a non-bridging oxygen. This fact cannot be neglected on account of the investigated glass containing high content of Al_2O_3. So we propose a new method to estimate the *NBO* content in this system glass, $\mathrm{NBO}=\sum Q^n(4-n)-[\mathrm{Al}]$. The fraction of non-bridging oxygen (NBO/NBO+BO), average number of NBO per tetrahedron (NBO/tetrahedron) can be described as follows:

$$\frac{\mathrm{NBO}}{\mathrm{NBO}+\mathrm{BO}} = \frac{\sum Q^n(4-n)-[\mathrm{Al}]}{\sum \mathrm{O}} \tag{6}$$

$$\frac{\mathrm{NBO}}{\mathrm{tetrahedrom}} = \frac{\sum Q^n(4-n)-[\mathrm{Al}]}{[\mathrm{Si}+\mathrm{Al}]} \tag{7}$$

Calculated and summarized in Table 4, the NBO/NBO+BO and NBO/tetrahedron both decreased with increasing the Al/Si ratio. In other words, this finding suggests an increase of glass network polymerization and/or a decrease of the disorder in the glass, which can answer for the viscosity increase in glass melts. However,

this disorder is preferred to the long-range disorder in structural network. We must make a distinction between this long-range disorder and the short-range disorder mentioned in Section 3.3. So we can make a conclusion that increasing Al_2O_3 substitute for SiO_2 leads to the number of NBO reducing and provides a more polymerized structure, with a related increase of the viscosity in glass melts.

5. Conclusions

Increasing Al/Si ratio on the viscosity, fragility and structure of a new float glasses of Na_2O–CaO–Al_2O_3–SiO_2 system were investigated, the conclusions can be drawn as follows:

a. The addition of Al_2O_3 substitute for SiO_2 in Na_2O–CaO–Al_2O_3–SiO_2 system glass increases the viscosity of glass melt and decreases the temperature interval of forming process in tin bath. The shortening of workability with increasing Al/Si ratios is mainly reflected in the viscosity interval of $10^{5.75}$–10^{10} Pa s. There is a negative correlation between the workability and the fragility index m. Comparing to the traditional float glass, the Na_2O–CaO–Al_2O_3–SiO_2 system glass melt has shorter workability and greater fragility.
b. Structural changes can be discerned in the Raman spectra: the Q^2 and Q^4 units are positively correlated with Al/Si ratio, whereas the Q^1 and Q^3 units both decrease with adding Al_2O_3. Some inferences have proved that the number of *NBO* reducing and a more polymerized structure with substitution of Al for Si are responsible for the increase of viscosity. The tetrahedral distortion, a decrease of Q^3/Q^2 in the Q^n species distribution, is also well correlated with an increase of the short-range disorder in the glass, responsible for the workability getting shorter and an increase of the fragility with adding Al/Si ratios.

References

[1] G.W. Morey, N.L. Bowen, The melting relations of the soda–lime–silica glasses, Journal of the Society of Glass Technology 9 (1925) 226.
[2] S. English, The effect of composition on the viscosity of glass: Part II, Journal of the Society of Glass Technology 8 (1923) 205–251.
[3] Bjorn Mysen, Structural behavior of Al^{3+} in silicate melts: in situ, high-temperature measurements as a function of bulk chemical composition, Geochimica et Cosmochimica Acta 59 (1995) 455–474.
[4] M. Bengisu, R.K. Brow, et al., Viscosity and glass transition temperature of hydrous float glass, Journal of Non-Crystalline Solids 353 (2007) 223–236.
[5] D. Giordano, M. Potuzak, et al., Viscosity and glass transition temperature of hydrous melts in the system $CaAl_2Si_2O_8$–$CaMgSi_2O_6$, Journal of Chemical Geology 256 (2008) 203–215.
[6] Pavel Hrma, Benjamin, et al., Viscosity of many-component glasses, Journal of Non-Crystalline Solids 355 (2009) 891–902.
[7] Mi-tang Wang, Jin-shu Cheng, et al., Effect of rare earths on viscosity and thermal expansion of soda-lime-silicate glass, Journal of Rare Earths 38 (2010) 308–311.
[8] P. Hrma, Glass viscosity as a function of temperature and composition: a model based on Adam–Gibbs equation, Journal of Non-Crystalline Solids 354 (2008) 3389–3399.
[9] Pavel Hrma, Arrhenius model for high-temperature glass-viscosity with a constant pre-exponential factor, Journal of Non-Crystalline Solids 354 (2008) 1962–1968.
[10] C.A. Angell, Relaxation in liquids, polymers and plastic crystals strong/fragile patterns and problems, Journal of Non-Crystalline Solids 131–133 (1991) 13–31.
[11] C.A. Angell, K.L. Ngai, G.B. McKenna, et al., Relaxation in glass forming liquids and amorphous solids, Journal of Applied Physics 88 (2000) 3113.
[12] R. Böh mer, C.A. Angell, Correlations of the non exponentiality and state dependence of mechanical relaxations with bond connectivity in Ge–As–Se supercooled liquids, Physical Review B 45 (1992) 10091–10094.
[13] E.M. Pierce, L.R. Reed, et al., Experimental determination of the effect of the ratio of B/Al on glass dissolution along the nepheline (NaAlSiO4)–malinkoite (NaBSiO4) join, Geochimica et Cosmochimica Acta 74 (2010) 2634–2654.
[14] R. Gresch, W. Muller-Warmuth, H. Dutz, ^{11}B and ^{27}Al NMR studies of glasses in the system Na_2O–B_2O_3–Al_2O_3, Journal of Non-Crystalline Solids 21 (1976) 31–40.
[15] H. Maekawa, T. Maekawa, K. Kawamura, T. Yokokawa, ^{29}Si MAS–NMR investigation of the Na_2O–Al_2O_3–SiO_2 glasses, Journal of Physical Chemistry 95 (1991) 6822–6827.
[16] G. El-Damrawi, W. Muller-Warmuth, H. Doweidar, I.A. Gohar, ^{11}B, ^{29}Si, ^{27}Al nuclear magnetic resonance studies of Na_2O–Al_2O_3–B_2O_3–SiO_2 glasses, Physics and Chemistry of Glasses 34 (1993) 52–57.
[17] Eric Le Bourhis, Glass: Mechanics and Technology [M], France, 2007, pp. 83–106.
[18] L. David Pye, Angelo Montenero, Innocent Joseph, Properties of Glass-Forming Melts [M], USA, 2005, pp. 75–138.
[19] Xiao Zifan, Cheng Jinshu, WU Hao, Effect of Al_2O_3/SiO_2 ratio on the viscosity and workability of high-alumina soda-lime-silicate glasses, Journal of the Chinese Ceramic Society 40 (7) (2012) 1000–1005.
[20] L.-M. Wang, Y. Tian, R. Liu, R. Richert, Structural relaxation dynamics in binary glass-forming molecular liquids with ideal and complex mixing behavior, Journal of Physical Chemistry B 114 (2010) 3618–3622.
[21] John C. Mauro, R.J. Loucks, Impact of fragility on enthalpy relaxation in glass, Physical Review E 78 (2008) 021502.
[22] C. John, Mauro. Effect of fragility on relaxation of density fluctuations in glass, Journal of Non-Crystalline Solids 357 (2011) 3520–3523.
[23] J. Deubener, H. Behrens, R. Müller, et al., Kinetic fragility of hydrous soda-lime-silica glasses, Journal of Non-Crystalline Solids 354 (2008) 4713–4718.
[24] Daniel R. Neuville, Viscosity, structure and mixing in (Ca, Na) silicate melts, Journal of Chemical Geology 229 (2006) 28–41.
[25] Daniel R. Neuville, et al., Role of aluminium in the silicate network: in situ, high-temperature study of glasses and melts on the join SiO_2–$NaAlO_2$, Geochimica et Cosmochimica Acta 60 (1996) 1727–1737.
[26] Mi-tang Wang, Jin-shu Cheng, et al., Raman spectra of soda–lime–silicate glass doped with rare earth, Phys. B 406 (2011) 3865–3869.
[27] J. Marchi, D.S. Morais, et al., Characterization of rare earth aluminosilicate glasses, Journal of Non-Crystalline Solids 351 (2005) 863–868.
[28] B.O. Mysen, et al., The role of aluminum in depolymerized, peralkaline aluminosilicate melts in the systems Li_2O–Al_2O_3–SiO_2, Na_2O–Al_2O_3–SiO_2 and K_2O–Al_2O_3–SiO_2, American Mineralogist 75 (1990) 120–134.
[29] Norimasa Umesaki, Masanari Takahashi, et al., Raman spectroscopic study of alkali silicate glasses and melts, Journal of Non-Crystalline Solids 205–207 (1996) 225–230.

[30] Jin Tan, Shanrong Zhao, et al., The effect of cooling rate on the structure of sodium silicate glass, Materials Science and Engineering B 106 (2004) 295–299.
[31] Bjorn O. Mysen, Olivine/melt transition metal partitioning, melt composition, and melt structure—Influence of Al^{3+} for Si^{4+} substitution in the tetrahedral network of silicate melts, Geochimica et Cosmochimica Acta 71 (2007) 5500–5513.
[32] N.M. Vedishcheva, et al., A thermodynamic, molecular dynamics and neutron diffraction investigation of the tetrahedral {Si(n)} species and the network modifying cation environment in alkali silicate glasses, Journal of Non-Crystalline Solids 867–873 (192) (1995) 292–297.
[33] N. Zotov, H. Keppler, The structure of sodium tetrasilicate glass from neutron diffraction, reverse Monte Carlo simulations and Raman spectroscopy, Journal of Physical Chemistry 25 (1998) 259–267.
[34] A.N. Cormack, J. Du, Molecular dynamics simulations of soda–lime silicate glasses, Journal of Non-Crystalline Solids 293–295 (2001) 283–289.
[35] James P. Hamilton, G. Carlo, Pantano. Effects of glass structure on the corrosion behavior of sodium-aluminosilicate glasses, Journal of Non-Crystalline Solids 222 (1997) 167–174.